Journal of Drug Delivery Science and Technology 88 (2023) 105001

Contents lists available at ScienceDirect

Journal of Drug Delivery Science and Technology

journal homepage: www.elsevier.com/locate/jddst

Polymeric complex nanocarriers of *Mangifera indica* gum & chitosan for methotrexate delivery: Formulation, characterization, and in vitro toxicological assessment

Sobia Noreen [a,b,**], Shazma Ehsan [a], Shazia Akram Ghumman [c], Sara Hasan [a,d], Fozia Batool [a], Bushra Ijaz [e], Bahareh Shirinfar [f], Khadeeja Ali Mohammed Alsader [g], Nisar Ahmed [g,*]

[a] Institute of Chemistry, University of Sargodha, Sargodha, 40100, Pakistan
[b] Department of Chemistry, University College London, 20 Gordon Street, London, WC1H 0AJ, UK
[c] College of Pharmacy, University of Sargodha, Sargodha, 40100, Pakistan
[d] Department of Chemistry, The University of Lahore, Sargodha Campus, Sargodha, 40100, Pakistan
[e] Centre of Excellence in Molecular Biology, University of the Punjab, Lahore, Pakistan
[f] Department of Chemistry, University of Bath, BA2 7AY, Bath, United Kingdom
[g] School of Chemistry, Cardiff University, Main Building, Park Place, Cardiff, CF10 3AT, United Kingdom

ARTICLE INFO

Keywords:
Mangifera indica gum
Chitosan
Methotrexate
Nanocarriers
In vivo toxicity
Antitumor effects

ABSTRACT

Methotrexate (MTX), a widely used chemotherapeutic drug, exhibits significant potential in the treatment of various solid tumors and hematologic malignancies. However, its therapeutic efficacy is often hampered by suboptimal pharmacokinetic profiles, causing drug resistance and a shortened plasma half-life. In recent years, in light of these challenges, a demand has arisen for novel strategies to augment the therapeutic potential of methotrexate. The present study presents an innovative approach in the development and evaluation of non-toxic nanocarriers designed for methotrexate delivery, using a biopolymer matrix comprised of *Mangifera Indica* gum (MIG) and chitosan (CS), employing the coacervation technique. The optimization process, guided by central composite design, was utilized to attain an optimal formulation containing 0.02% w/v% MIG and 0.01% w/v% CS. The characterization of optimized formulation revealed smooth, spherical nanoparticles (229.7 nm diameter, PDI 0.296) with 69.5 ± 2.0% entrapment efficiency. Additionally, a pH-dependent sustained release of the MTX for up to 24 h was found using in-vitro drug release analysis. Furthermore, the optimized formulation displayed significant cytotoxic effects in an MTT assay, highlighting its potential as an effective carrier for the delivery MTX to cancer cells. These findings offer valuable insights into pH-responsive drug delivery to tumor cells and underscore the promising therapeutic efficacy of MIG/CS nanoparticles, positioning them as a compelling option for novel pharmaceutical formulations.

1. Introduction

Cancer, a condition originating from genetic changes at the molecular level, leads to unchecked cell proliferation and tissue dysfunction. Although chemotherapy serves as a prevalent primary therapy, it confronts challenges such as restricted drug solubility, numerous unavoidable side effects and the development of drug-resistant cancer cells [1]. Methotrexate (MTX; amethopterin; 4-amino-10-methylfolic acid), an early anticancer drug used in the treatment of solid tumors, inflammatory disorders and hematological malignancies, has demonstrated inherent limitations, notably its weak targeting proclivity, leading to various adverse side effects like baldness, nausea, body pains, hepatotoxicity, and myelosuppression [2,3]. Addressing this quandary, a promising approach emerges through the nano-scaling and encapsulation of anticancer agents within stimuli-responsiveness carriers that are capable of facilitating endosomal absorption and tailored cargo delivery to tumor cells in response to specific triggers, including pH, hypoxia and over-expressed enzymes [4–6] Furthermore, the efficacy and precision of anticancer drug distribution are significantly enhanced via these stimuli-responsive nanocarriers, which selectively release therapeutic

* Corresponding author. School of Chemistry, Cardiff University, Main Building, Park Place, Cardiff, CF10 3AT, United Kingdom.
** Corresponding author. Institute of Chemistry, University of Sargodha, Sargodha, 40100, Pakistan.
E-mail addresses: sobia.noreen@uos.edu.pk (S. Noreen), AhmedN14@cardiff.ac.uk (N. Ahmed).

https://doi.org/10.1016/j.jddst.2023.105001
Received 21 August 2023; Received in revised form 22 September 2023; Accepted 24 September 2023
Available online 26 September 2023

agents at tumor sites. Studies have shown that nanoscale drug delivery systems, especially those responsive to tumor microenvironments, have the potential to reduce systematic toxicity and enhance therapeutic outcomes in cancer treatments. Concurrently, the landscape of nanotechnology research has swiftly transposed towards the use of cost-effective biopolymers, such as lipids and polysaccharides, in nanocarrier fabrication [7]. Carbohydrates, proteins and lipids, as polymeric materials, play pivotal roles in formulation due to their exceptional capacity for water and biological substances absorption and retention [8]. Moreover, due to their small nanometer dimensions, polymeric nanoparticles (PNPs) have the potential to deliver therapeutic substances efficiently by changing their formulation to get the desired result [9,10]. Additionally, the eco-friendly nature of biopolymer nanoparticles, instead of other synthetic carriers, namely metal nanoparticles reduces pollution by minimizing metal contamination, advocating their use in pharmaceutics [11–13].

Different biopolymers (natural and synthetic) have been utilized therapeutically or as adjuvants in the treatment of cancer, displaying significant potential to reduce the perils associated with conventional therapies while simultaneously enhancing therapeutic efficacy and minimizing side effects [14]. However, for the majority of patients, synthetic polymer based medications, for instance, PLGA-based LAI (long acting injectable) medication are rather pricey [15]. Even though many of these PLGA-based LAI medication products have fallen off-patent or are non-exclusive, there is no generic version of these drugs on the market [16]. The high cost of synthetic polymer based medication has led to an exploration of natural biopolymers, specifically polysaccharide constituted plant gums, as cost-effective alternatives [17]. This interest in polysaccharide constituted plant gum utilization in nanoparticle formulations is owed to numerous benefits, like biocompatibility, biodegradability, and very low toxicity [18–20]. Furthermore, the synthesis of nanoparticles by using natural biopolymers is a cost-effective, convenient and environmentally safe approach, as the non-biological techniques, such as chemical and physical approaches, are seriously hazardous and highly toxic to biological entities [21]. A variety of plant gums have been utilized for encapsulation of MTX in conjunction with chitosan. When coupled with chitosan, these plant gums have been shown to play a significant role in advancing drug carriers, holding a promise to enhance the therapeutic effectiveness of MTX based treatments [14].

Mangifera indica gum (MIG), a dried adhesive polysaccharide plant gum, has showcased significant promise across various biomedical domains. It is extracted from the bark of *Mangifera indica* L., (commonly known as mango), a significant fruit crop grown in more than 100 tropical and subtropical countries. It has a chromosome number of 40 and belongs to the Anacardiaceae family and the Sapindales order [22]. These trees have a lengthy lifespan, and some have been producing fruit for almost 300 years. MIG is systematically extracted from mango plant bark, which initially involves the careful removal of a portion of tree bark from trunk and branches. Over the course of several days to weeks, the gum spontaneously exudates and solidifies on the inner layers of the exposed bark. Once it reaches the desired consistency, the gum is collected, cleaned and processed to remove impurities [23]. Moreover, MIG has several intriguing properties, including its ability to firm gels at low concentrations and its carbohydrate content of 33.68% determined via proximate analysis. Further analysis through GC-MS of the aqueous MIG extract, has revealed the predominant sugars: galactose, glucose, and arabinose, with respective concentration of 839.7, 495.6 and 483.7 mg/100 g dry weight. Additionally, a low concentration of fructose at 155.9 mg/100 g has also been detected [24]. Numerous studies have been conducted on this gum to determine its binding, sustained release, and dissolving properties [25].

Chitosan (CS), a copolymer of D-glucosamine and N-acetyl-D-glucosamine, is derived from the deacetylation of chitin extracted from a variety of sources, including crustaceans, insects, mollusks, fungi, and shrimp [26,27]. Additionally, it serves as a nanofiller in films for active packaging [28]. It is regarded for its antibacterial and antioxidant properties, as well as its potential as a biodegradable, biocompatible, and non-toxic nanocarrier for pharmaceuticals and other biomedical applications [29,30]. Because of its cationic properties, chitosan promotes bioavailability by speeding up blood circulation and boosting drug permeability by loosening tight connections between epithelial cells [31]. Chitosan nanoparticles can be created using a variety of techniques, the two most popular of which are polyelectrolyte complexation and ionic gelation [32]. When opposingly charged macromolecules, such as drug polymers, polymer-polymers, or polymer-drug-polymers, interact, polyelectrolyte complexes are formulated [33,34]. Chitosan has been used in several studies to generate nanosized delivery vehicles with anionic polymers like sodium alginate, pectin, reduced albumin, glycol, and tripolyphosphate [35]. These experiments have shown that it is conceivable to transport drugs to definite cellular regions over an extended period of time [36–39]. Mango tree bark gum and chitosan nanoparticles are promising nanocarriers with potential applications in drug delivery, imaging, and tissue engineering. Their biocompatibility, biodegradability, and low toxicity make them an attractive alternative to synthetic polymers, and their mucoadhesive properties can enhance drug absorption and retention in the gastrointestinal tract.

The aim of the current study is to fabricate, optimize and characterize the biopolymeric nanocarriers of MIG/CS and MTX for anticancer drug delivery with efficacious and sustained delivery potential. It also includes characterizing the architectural makeup of manufactured nanoparticles and determining their size, yield and encapsulation effectiveness in all formulations. The current study specifies the self-assembly method for fabricating nanoparticles, which uses block copolymers made of two polymer chains differing in hydrophilicity. The coacervation approach has been used to achieve sustained drug release inside cancer cells and to improve pharmacokinetic characteristics. To the best of our knowledge, this was the first attempt to investigate the formulation of CS-MIG polyelectrolyte-stabilized nanosuspensions for therapeutic applications. The structure of polyelectrolyte stabilized nanoparticles' effects on human cancer cells is little known. The purpose of this study was to see how spherical nanoparticles affected human Hep G2 cancer cell lines. The study's findings will very certainly provide basic parameters for the design of cancer delivery systems.

2. Material and methods

2.1. Materials

Chitosan with a medium molecular weight and a deacylated content of 75–85% was purchased from S Sigma-Aldrich (GmBh Chemie, Germany). The Peshawar-based pharmaceutical offered methotrexate as a gift. Ethanol, sodium hydroxide, glacial acetic acid >99.7%, mango plant powder, dimethyl sulfoxide (DMSO) and other chemicals and reagents were purchased from Sigma-Aldrich (GmBh Chemie, Germany) and Fisher Scientific, UK, for use in the current investigation. Only analytical-grade substances were used, and all solutions were made with deionized water.

2.2. Extraction of gum from Mangifera indica bark exudates

The extraction of gum commenced by making incision in the stem bark of *Mangnifera indica* trees. Subsequently, through careful scratching, the gum was extracted from the bark and subjected to thorough cleansing to eliminate impurities, following which it was subjected to drying. This dried gum was subsequently pulverized into a fine powder. To achieve further refinement, a micro-sieve was employed to meticulously segregate the gum powder. The obtained sample was stored in sealed glass vials, safeguarded at room temperature, for subsequent analysis. The dehydrated gum, weighing 150 g, was immersed in 500 mL of deionized water and homogenized, followed by 8 h of stirring at

ambient conditions. Utilizing centrifugation, the transparent upper liquid layer was separated, and the resulting mucilaginous solution was filtered via muslin cloth. Additionally, to remove undesirable constituents, the filtrate was subjected to precipitation process by adding twice the original amount of ethanol. This method yielded precipitates, which were duly collected, dried, and subsequently ground into a fine powder. This powdered gum was further refined by sieving via a no. 80 filter. The resultant gum was carefully preserved in an airtight glass container to facilitate further analysis [23,40]. The extraction yield of MIG was calculated by equation (1).

$$\text{Extraction yield } (\%) = \frac{Mucilage\ weight\ (g)}{Raw\ material\ weight\ (g)} \text{ x } 100 \quad (1)$$

2.3. Formulation of nanoparticles

MTX loaded MIG-CS nanoparticles (MIG-CS NPs) were developed using an earlier published coacervation process with minimal modifications, preceded by ultra-sonication. Using the varying ratios of MIG, CS, and MTX, MTX loaded MIG-CS NPs were fabricated, as shown in Table 1. Two separate solutions were prepared: a 100 mL MIG solution and a 100 mL CS solution, using distilled water and 2.5% glacial acetic acid, respectively. The MIG-solution was added to the CS-solution followed by stirring for an additional 20 min at 40 °C and an additional 5 min at 50 °C. Acetone was used as the solvent to make a solution of MTX (1 μg/1 mL). Furthermore, MTX (10 mg) was dissolved in 10 mL of acetone which was then serially diluted to achieve a concentration of 1 μg/mL. Using a nano-syringe, the MTX-solution (5 mL) was then introduced dropwise in MIG-CS solution and the MTX containing MIG-CS solution was stirred for 45 min at 65 °C. After cooling the sample to 35 °C, it was placed in an airtight container. No washing was done because the end result was a nanosuspension [41].

2.4. Factorial design

The prepared MTX loaded MIG-CS formulations were optimized using a 3-level 2-factor central composite design (CCD) based on response surface methodology (RSM). Preliminary studies and published literature were used to select independent factors and dependent factors [42,43]. Based on previously reported literature and initial experiments, key factors influencing the MIG-CS NPs efficacy were identified. The concentration of MIG and CS was set in range of 0.02–0.04 w/v% and 0.01–0.03 w/v% respectively, as preliminary trials suggested this range to provide precise control over the nanoparticle's properties, including particle size and encapsulation efficiency [1,14]. Particle size is crucial for tissue penetration while encapsulation efficiency ensures effective drug delivery [44]. Initial trials demonstrated that altering the concentration of both MIG and CS had noticeable effect on both particle size and encapsulation efficiency, consistent with previous studies carried out on plant gum-chitosan based nanoparticles [14,45]. Nine formulations with varying concentrations of MIG and CS were suggested by Drug Design Expert (DES) software, shown in Table 1. Particle size (R1) and encapsulation effectiveness (R2) were chosen as dependent parameters, whilst chitosan (CS) and mango plant gum (MIG) concentrations were selected as independent variables. All formulations maintained a constant drug concentration i.e., 1 μg/mL. The mean values of each formulation were calculated three times, and they were then used to fit the results into a variety of mathematical models, such as cubic, linear, quadratic, and 2FI. Based on the modified R2, predicted R2, p-value, and residual sum of squares, a significant model was chosen. The relation between the factors and the responses was assessed using a generalized quadratic equation (1). The formulation with the best optimal responses was obtained using the desirability parameter. The statistical model was validated using an ANOVA [46].

Table 1
The independent factors and dependent variables obtained by 2^3 CCD in DES.

Std	Run	Factor 1	Factor 2	Response 1	Response 2
		X1	X2	Y1	Y2
		MIG (w/v %)	CS (w/v %)	Particle size (nm)	Encapsulation efficiency (%)
2	**1**	0.04	0.01	355.5	78.3
6	**2**	0.04	0.02	364.77	79.45
3	**3**	0.02	0.03	344.45	74
10	**4**	0.03	0.02	326.45	75.89
1	**5**	0.02	0.01	231.3	71.9
11	**6**	0.03	0.02	326.45	76.1
9	**7**	0.03	0.02	326.87	76.5
5	**8**	0.02	0.02	287.34	72.89
4	**9**	0.04	0.03	376.34	80.8
7	**10**	0.03	0.01	295	75.3
8	**11**	0.03	0.03	361.34	77.34

$$Y = b_o + b_1 X_1 + b_2 X_2 + b_{11} X_1^2 + b_{22} X_2^2 + b_{12} X_1 X_2 \quad (2)$$

where Y = response; X1 = MIG concentration; X2 = CS concentration; bo = intercept; b1 and b2 = co-efficients; X12/X22 = second order effects of MIG and CS concentrations respectively; X1X2 = interactive effects of excipients concentrations.

2.4.1. Mean particle diameter as Y1

Using a Zetasizer, the particle size of MTX-MIG-CS NPs was determined at room temperature (Malvern Instruments, model no. 2000). Particle size investigations in concentrated liquids are inaccurate mostly because of multiple scattering. The size of suspended particles is often measured using diluted solutions to limit the chance of inaccurate measurement [47]. In order to prevent inaccurate measurements, a diluted solution of 1% was used for the analysis [48].

2.4.2. Drug encapsulation efficiency (DEE %) as Y2

One of the key elements to confirming the encapsulation process is encapsulation efficiency. However, the technology used affects the effectiveness of encapsulation (for example, in terms of survival rate or release) [49,50]. It is crucial that the encapsulating method can include an increased concentration of drug. The approach that is frequently employed is the degradation of the carriers through centrifugation, followed by the dissolution of the delivery carriers in phosphate buffer solution; PBS and the detection of the drug using spectroscopic techniques. In present study, UV-Spectrophotometer (Shimadzu, Japan) was employed to calculate the degree of entrapment. At 4 °C, 10 mL of the produced nanosuspension was centrifuged for 45 min at 10,000 rpm. The supernatant was gathered in order to measure UV absorbance at 303 nm and determine the amount of free MTX in the formulations. With its 10, 20, 40, 60, 80, and 100 L/mL solutions, a standard calibration curve for MTX solution was produced at 303 nm [51]. Equation (3) was used to determine the drug entrapment/encapsulation efficiency.

$$\text{DEE } (\%) = \frac{\text{Total drug} - \text{Free drug}}{\text{Total drug}} \times 100 \quad (3)$$

2.4.3. Optimization of formulation

The desirability approach was applied to the optimization of microsphere formulations using both mathematical and graphical techniques. A model was established by DES in order to arrive at a suitable collection of independent criteria for maximizing all responses. Value restrictions such as maximum, minimum, and range were used to calculate desirability/D, which produced a graph of desirability where D stands for the mean of the dependent variables proposed by the software. We choose the parameter that, within a certain range, generated the smallest PS (nm) and DEE (percent). In order to get the best PS (nm) and DEE (%) for the effective optimization of MTX-MIG-CS NPs (F0), a comparison between actual and anticipated values was also done [46].

2.4.4. Optimized MTX loaded MIG-CS NPs (F0) characterization% yield and %drug content

The F0 NPs were centrifuged in a microcentrifuge to collect the supernatant and pellets for calculating the percentage drug content and yield. At a cooling temperature of 5.0 °C, centrifugation was conducted for 60 min at a speed of 10,000 rpm. In this experiment, the supernatant was discarded, and the pellets were left to dry [52]. The following equations (4) and (5) were used to calculate the weights of pure MTX, MIG, CS, and MIG-CS NPs that were loaded with MTX.

$$\%\text{Drug Content} = \frac{\text{Entrapped MTX}}{\text{Weight of NPs}} \times 100 \tag{4}$$

$$\%\ \text{Yield} = \frac{\text{Weight of NPs}}{\text{Weight of total solid (MIG + CS + MTX)}} \times 100 \tag{5}$$

2.4.5. Fourier Transform Infrared Spectrophotometer (FTIR) analysis

Using an IR Prestige-21 spectrophotometer, spectral analyses of F0; MTX loaded MIG-CS NPs, natural polymers (MIG and CS) and the drug; MTX were performed (Shimadzu, Japan). This investigation was conducted to find possible interactions between drug and polymeric excipient [52,53].

2.4.6. Particle morphology analysis

Scanning electron microscopy; SEM (JSM-IT100, Jeol, Tokyo, Japan) at 1000 magnification was utilized to examine the morphology of MTX loaded MIG-CS NPs. Samples were gold-sputtered coated after being placed on aluminum stubs. Each sample was ultra-centrifuged, dried until all solvent was removed, and then washed with water [54].

2.4.7. In-vitro drug release study

The MTX release rate was analysed using a diffusion approach in a dissolution apparatus. The samples (5 mL) were suspended in PBS solutions with pH values ranging from 7.4 to 1.2 in a diffusion bag. The 200 mL of PBS solutions with pH values of 7.4, 6.8, and 1.2 were also added to the dissolving apparatus cells, which were heated to 37 °C and stirred continuously at 100 rpm. A 5 mL sample was taken at regular intervals of 30 min, 45 min, 1, 2, 3, 4,5, 6, 8, 10, 12 and 24 h, with new buffers being used to replace the removed volumes. The concentration of MTX in F0 NPs was determined by measuring the absorbance using a UV-spectrophotometer at 304 nm in contrast to a blank and using the calibration curve for pure MTX [54].

2.4.8. Kinetic studies of drug release

To ensure that the MTX was being released from the NPs in the most efficient manner, several kinetic models were utilized to profile the dissolution of MTX-loaded MIG-CS NPs [55]. These are the models:

Zero Order model: This model's main use is to explain the concentration-independent release rate of MIG-CS NPs that are loaded with MTX, as shown by equation (6).

$$Q_t = Q_0 + K_0 \,.\, t \tag{6}$$

Where Q0 is the initial quantity of drug present in solution and Qt is the amount of drug released during time t.

First Order model: In according to equation (6), this model examines the hydrophilic drug release from a porous matrix as opposed to the drug content within the drug carrier.

$$LogQ_t = LogQ_0 - \frac{K_1}{2.303}\, t \tag{7}$$

Where Q_t is the amount of drug dissolved at time t; Q0 is the initial drug amount in solution and K1 is the first-order rate constant.

Higuchi model: This model is commonly used to represent the cumulative percent release of hydrophilic drugs from hydrophobic polymeric matrixes in proportion to the square root of time, as shown in equation (8).

$$Q_t = K_H\, t^{\frac{1}{2}} \tag{8}$$

Where K_H is higuchi model's constant and Q_t is the amount of drug dissolved at time 't'.

Korsmeyer–Peppas model: In according to equation (9), this model is often utilized to evaluate the mechanism underlying the cumulative drug release integrated into polymeric matrixes.

$$\frac{M_t}{M_\infty} = K_r t^n \tag{9}$$

Where $\frac{M_t}{M_\infty}$ is the drug fraction release at time "t" and K_r is the release constant and n is the release mechanism dependent exponent

Hixson-Crowell model: The Hixson-Crowell law describes the release from systems when there is a change in particle surface area and diameter (equation (10)).

$$Q_{01/3} - Q_{t1/3} = K_{HC}.t \tag{10}$$

Where k_{HC} is an integral surface volume relationship constant.

2.5. Hemolytic studies

The interaction between fresh blood and F0 NPs was used to quantify hemolytic activity. In tubes filled with heparin, 5 mL of brand-new whole human blood was taken. At 3000 rpm for 15 min, the blood was centrifuged. After the serum had been separated and was used as the positive control, red blood cell pellets were three times washed with PBS that had a pH of 7.4. To create the negative control, the solution was diluted with distilled water. Further dilution with PBS was done using the acquired red blood cells (2 mL). The formulations were incubated and centrifuged at 3000 rpm for 10 min at concentrations of 0.05 mg, 0.025 mg, and 0.01 mg. The formulations prepared were used to determine the absorbance by UV-Spectrophotometer (PEAK Instruments) at 540 nm [56,57]. % hemolysis was based on equation (11).

$$\%\ \text{Hemolysis} = \frac{\text{Abs (sample)} - \text{Abs (Blank PB)}}{\text{Abs (positive control)} - \text{Abs (negative control)}} \times 100 \tag{11}$$

2.6. In vitro cell viability study via MTT assay

For this study, Hep G2 cell growth was regulated by the metabolism of the tetrazolium substrate MTT(3-[4,5-demethyliazol-2-yl]-2,5 diphenyl tetrazolium bromide). The test sample was made in a 1:1:1 ratio using MTX, blank MIG-CS NPs, and F0. The test materials were dissolved in 500 g/mL of dimethyl sulfoxide (DMSO), diluted with water to 200 g/mL, and then frozen for later use. After defrosting, the frozen concentration (200 g/mL) was diluted with NP concentrations that were progressively lower before being grown on culture plates for 48 h. The cell lines were grown in DMEM (Dulbecco's Modified Eagle Medium), which contains 10% FBS and four times as many minerals and amino acids (Fetal Bovine Serum). The cells were inserted at 37 °C with a CO2 atmosphere of 5%. A 96-well plate was seeded with 10,000 Hep G2 cells per well and left for 24 h. The cells were subsequently cultured for 12 and 24 h with test solutions added to the medium in varied doses. The medium was taken out and incubated for 4 h with MTT solution at 5 g/L in PBS at a pH of 7.4. There was no longer any growing medium, so 150 L of DMSO were added. The plate was gently agitated after the formazan precipitate had been dissolved [58]. At 570 nm, the absorbance was measured. Reduced absorption implies decreased cell viability [59]. The experiment was carried out in triplicate, and the findings (equation (12)) are shown as the mean standard deviation.

$$\text{Cell viability} = \text{Test cells (abs)} \,/\, \text{Control cells (abs)} \times 100 \tag{12}$$

2.7. Acute in-vivo toxicity analysis

Adult male albino mice (*Mus musculus*) weighing 26–28 g and aged 8–10 weeks were purchased from the University of Veterinary Sciences, Sargodha for use in this study. They were kept in the zoology department's animal home at the University of Sargodha. They were raised in plastic cages with bedding that was lined with steel wire gauze and trimmed with fine wood. Temperature (25 °C 3 °C), humidity (45%), and a 12-h cycle of light and darkness were provided in the animal housing. Water and standard mouse feed were offered. Mice received an experimental dose of MIG-CS NPs in accordance with excipient toxicity testing guidelines through an oral route using metal gavages once after a week of acclimatization lasting for 21 days [60]. During the investigation, changes in body weight, mortality, survival, and other clinical parameters were noticed. Mice were dissected on day 22 of the experiment to collect blood for organ testing [61].

2.8. Statistical analysis

The standard deviation was calculated using the average findings after three rounds of testing for each test. The R^2 and MSC of several kinetic models were examined using the DD-Solver program on drug release data to assess their accuracy and predictability.

3. Results and discussion

The pivotal concerns in cancer therapy encompass limited absorption and compatibility with normal cells. The utilization of proficient techniques, namely coacervation and employing biopolymers to encapsulate cancer drugs, presents a promising avenue to address these limitations. Coacervation, an economical and non-toxic method, involves the formation of liquid-liquid phase separation in a polymer solution to form coacervate droplets encapsulating a core material. Its merits encompass high encapsulation efficiency, controlled release, versatility for various therapeutic agents and protection of encapsulated materials from external factors. Nonetheless, despite its unique advantages, co-acervation can be a complex process that demands a considerable amount of biopolymer and may exhibit limited compatibility with core polymers [62,63]. In the present study, with MIG extraction yield of 28.76%, the biopolymers i.e. MIG and CS were selected as nanocarriers for MTX administration. Owing to their non-toxic, biodegradable, low production cost-requiring and easy scalability, allowance favoring pharmaceutical economics. Additionally, a synergy interaction emerged because of formation of polyelectrolyte complexes between MIG and CS, where the former was used as anionic and the latter one was employed as cationic polymer for MTX encapsulation via coacervation technique, which is illustrated in Fig. 1.

3.1. Experimental design and optimization

The use of statistical technique known as central composite design empowers researchers to concurrently investigate the intricate interplay between multiple factors and their subsequent impact on dependent variables [64]. This statistical optimization accelerates optimization test by performing virtual screening, predictive modeling besides streamlining best formulation selection while reducing hit and trail errors which ultimately shortens the drug development timeline. In the present study, 2^3 central composite design was used to optimize the MIG-CS NPs experimental design. Table 1 succinctly outlines the software's recommended 9 runs, delineating the concentrations of MIG and CS as independent variables and corresponding particle size (PS in nm) and encapsulation efficiency (%DEE) as the responses. The validation of statistical models was facilitated by one-way ANOVA (Table 2). Furthermore, to elucidate the correlation between distinct factors and responses, response surface methodology (RSM) was employed as a result of which 2D contour graphs and 3D response surface graphs were constructed, as shown in Figs. 1 and 2. Employing DES for statistical analysis, observed values from 9 experimental batches were fitted into various models, encompassing linear, two-factor interaction, quadratic and cubic models. The selection of polynomial model was predicated on statistical matrices including the correlation coefficient (R^2), expected R^2, adjusted R^2 and predicted residual sum of squares (PRESS). The PS (nm) response for MTX-loaded MIG-CS conformed to a quadratic model, %DEE exhibited a robust alignment with linear response. The statistical significance of quadratic and linear models, was evidenced by the F and p-values, was particularly pronounced for both PS (nm) and %DEE, reflecting an optimum goodness of fit for both responses. Notably, the coefficient of variance (C.V.) values and precision indices of the selected models denoted substantial repeatability and signal strength, respectively. The non-significant lack of fit values for both responses underscored the models' fit to the experimental data [41,65].

3.1.1. Particle size in nm as Y1

To determine the size distribution of MTX loaded MIG/CS NPs, the study used the z-average measurement. The results showed that the developed nanoparticles had an average diameter ranging from 231.3 to 376.34 nm, indicating that they were nanometers in size. The DDE software was used to construct a polynomial equation that related the independent variables of MIG and CS to the particle size. Equation (13) showed that the independent variables had a direct impact on particle size, with MIG concentration having the most significant effect. equation (13) and Fig. 2 were acquired from DES with coded coefficients. equation (13) showed that an increment in particle size is greatly influenced by polymers blend solution. Furthermore, Fig. 1 (a, b, and c) showed the relationship between MIG and CS concentrations and how changes in their concentrations affected particle size [66,67].

$$PS\ (nm) = 1.20 + 9061.29X1 + 9785.35X2 - 2.30x105X1X2 - 9231.58 \times 1^2 + 11918.42 \times 2^2 \quad (13)$$

3.1.2. Drug encapsulation efficiency as Y2

The entrapment efficiency of MTX loaded MIG/CS NPs was investigated via response surface methodology by DES aid to establish a relationship between the independent variables i.e. concentrations of MIG and CS and response (%DEE). The observed range of entrapment efficiency values, presented in Table 1, varied between 71.9% ± 1.2% and 80.8% ± 1.3%. The polynomial equation (14) was utilized to model the relationship between the independent variables of MIG and CS and the entrapment efficiency.

$$DEE\ (\%) = 64.85 + 329.54X1 + 34.14X2 + 1000X1X2 - 336.84 \times 1^2 + 1163.16 \times 2^2 \quad (14)$$

The DES software was used to construct equation (14) and the results

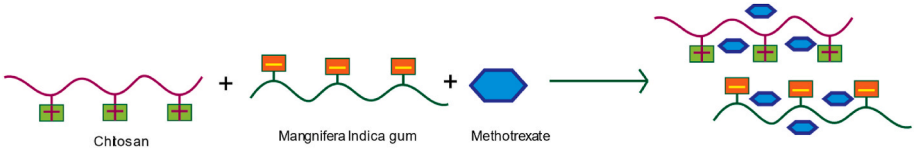

Fig. 1. Schematic representation for the formation of nanosized polyelectrolyte complexes.

Table 2
ANOVA results for dependent variables.

Response 1 (Quadratic Model)						
Source	Sum of Squares	df	Mean Square	F-value	p-value	
Model	17912.17	5	3582.43	24530.39	<0.0001	significant
A/X1	533.97	1	533.97	3656.28	<0.0001	
B/X2	1096.52	1	1096.52	7508.31	<0.0001	
AB/X1X2	2130.28	1	2130.28	14586.93	<0.0001	
$A^2/X1^2$	2.16	1	2.16	14.78	0.0121	
$B^2/X2^2$	3.60	1	3.60	24.64	0.0042	
Residual	0.7302	5	0.1460			
Lack of Fit	0.6126	3	0.2042	3.47	0.2316	not significant
Pure Error	0.1176	2	0.0588			
Cor Total	17912.90	10				
Response 2 (Linear Model)						
Model	72.50	5	14.50	331.28	<0.0001	significant
A/X1	0.7062	1	0.7062	16.14	0.0102	
B/X2	0.0133	1	0.0133	0.3050	0.6046	
AB/X1X2	0.0400	1	0.0400	0.9139	0.3830	
$A^2/X1^2$	0.0029	1	0.0029	0.0657	0.8080	
$B^2/X2^2$	0.0343	1	0.0343	0.7831	0.4167	
Residual	0.2188	5	0.0438			
Lack of Fit	0.0268	3	0.0089	0.0930	0.9572	not significant
Pure Error	0.1921	2	0.0960			
Cor Total	**72.72**	**10**				

Model Statistics	Source	Sequential p-value	Lack of Fit p-value	Adjusted R^2	Predicted R^2	
Response 1	Quadratic	0.0070	0.2316	0.9999	0.9997	Suggested
Response 2	Linear	<0.0001	0.9590	0.9950	0.9935	Suggested

indicated that MIG concentration had the most significant impact on % DEE. The coefficients of the model terms showed that the individual impact of X1 and X2 had a positive effect on %DEE, while the squared impact of X1 had negative whereas X2 had a positive effect on %DEE. Moreover, Fig. 3 (a, b, and c) illustrated the relationship between MIG and CS concentrations and their impact on %DEE. It was found that % DEE decreased with an increase in CS concentration at low levels of MIG concentration but remained constant at high levels of MIG concentration. These results are consistent with previous studies that have shown the importance of independent variables in determining the properties of NPs [66,67].

3.1.3. Formulation optimization

The DES used 9 separate sets of data to construct an algebraic solution that resulted in an optimized formulation for MTX-loaded MIG/CS NPs that had desirable properties, as shown by the formulation's highest desirability of 0.998. The values of independent variables were limited to a range of 0.02–0.04 w/v% for MIG and 0.01–0.04 w/v% for CS to produce optimal responses i.e. PS (nm) and %DEE with individual desirability of 0.98 and 1 respectively. The values derived from the desirability function were compared with the actual experimental results after an optimized formulation (F0) was generated under the constrained conditions. The computed relative error between the experimental values and the projected values is shown in Table 3. The study's finding that the software is highly predictable and robust in optimizing MTX loaded MIG/CS NPs by the low size of relative error that was discovered [68]. Additionally, Table 3 presents a comparative analysis of various nanoformulations designed for drug delivery. In comparison to these nanocarriers, the optimized MIG-CS NPs stands out as a potential candidate for efficaciously delivering MTX to target site, primarily due to favourable atribuet namely, particle size and encapsulation efficiency.

3.2. Characterization of optimized MIG-CS formulation

3.2.1. Fourier Transform Infrared Spectrophotometer (FTIR) spectral analysis

With the use of Fourier Transform Infrared Spectrophotometer (FTIR) analysis, we investigated the functional groups to determine the electrolytic binding existing in between the MTX loaded MIG-CS NPs (Fig. 4).

The FTIR spectrum of CS exhibited distinctive peaks at 3325.28 cm^{-1}, 2862.36 cm^{-1}, and 2818 cm-1, which correspond to the –OH, -CH2, and -CH3 groups, respectively. A distinctive adsorption band for the amino group was in the 3901.99 cm^{-1} range. There were two amide bands at 1610.56 and 1581.63 cm^{-1}, respectively. The NH- bending vibration and primary alcohol's –OH group were visible in the peaks at 1527.62 and 1456.26 cm^{-1}. C–O stretching was visible at the peak at 1031.92 cm^{-1}.

The FTIR spectrum of the active MTX showed absorption peaks at 3766.98 cm^{-1} and 3564.45 cm-1 demonstrating the existence of imines and the –OH group respectively. Alkyl groups, aromatic groups, carboxyl groups were present at peaks 3323.35 cm-1, 2937 cm-1, and 1870.95 cm-1 respectively. C═C was present in the aromatic ring as evidenced by absorption peak presence at 1492.9 cm^{-1}.

The FTIR spectrum of pure MIG showed absorption peaks at 3809.41 cm^{-1} and 3662.82 cm^{-1} indicating sharp O–H bond stretching for the presence of alcohol. The peak at 3273.2 cm^{-1} also indicated O–H bond stretching (alcohol). The absorption peaks of 2872.01 cm^{-1} and 2723.49 cm^{-1} in the frequency range of 3000–2500 cm^{-1} indicated C–H bond stretching of alkane and aldehyde respectively. The peaks in the frequency range of 2400–2000 cm^{-1} indicated the presence of functional groups i.e., O═C═O (CO2), and N═C═O (isocyanate). The frequency range of 2000–1650 cm^{-1} indicated C═O bond stretching. The absorption peaks in the frequency range of 1400–1000 cm^{-1} showed O–H bending (either carboxylic acid or alcohol).

The FTIR spectrum of MTX-loaded NPs containing a mixture of CS, MIG, and drug i.e., MTX shows a peak at 3599.17 cm^{-1} indicating a sharp O–H stretching bond of alcohol. The bands of absorption at 3182.55 cm^{-1} and 3167.12 cm^{-1} indicated O–H bonding of carboxylic acid. The peak at 2131.34 cm^{-1} and 1656.85 cm^{-1} shows weak C═C stretching bond (monosubstituted alkyne) and C═N stretching respectively. The bands at 1421.54 $cm^{-1}$and 1408.04 cm^{-1} indicate O–H bending (carboxylic acid). The peaks at 1305.81 cm-1, 987.55 cm^{-1}, and 788.89 cm^{-1} indicate the presence of strong S═O stretching (sulfone), strong C═C bending (monosubstituted alkenes), and medium C═C bending (trisubstituted alkene).

The overlaid FTIR spectrum of MTX, MIG, Chitosan, and drug-loaded

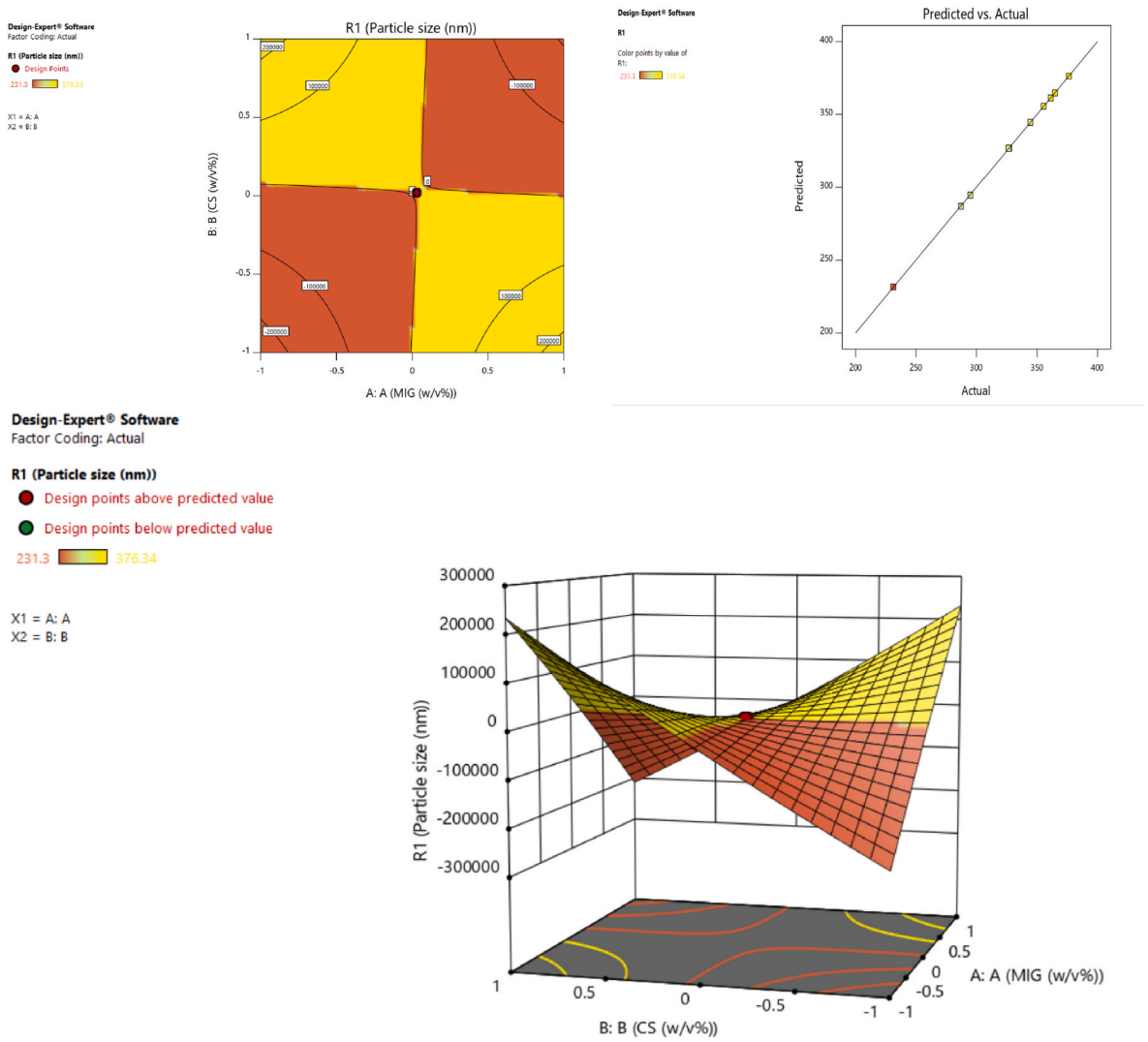

Fig. 2. 2-D contour surface predicted vs actual and 3-D response graphs illustrating the influence of MIG and CS content on PS (nm) of MIG/CS NPs.

nanoparticles show the presence of O–H stretching bands indicating the presence of hydrogen bonding, cumulative C═C and C═O stretching bonds, and carbonyl stretching bonds in chitosan and methotrexate affirming the formation of polyelectrolytic complex of MIG-CS encapsulating MTX [72].

3.2.2. % DEE, %drug content and % yield calculation

The obtained % DEE of F0 was 69.5 ± 2.0%. The % yield of F0 was estimated to be 69.7 ± 2.0%, with the percentage drug content being 71.4 ± 2.0%. It can be said that the higher the concentration of plant mucilage used higher the entrapment efficiency of the drug used [73]. The characterization of formulations for percent yield, percent drug content, and percent encapsulation efficiency is shown in Table 4.

3.2.3. Particle size and morphology analysis

Nanosized drug delivery carriers exhibit improved therapeutic potential, enabling enhanced interaction within tumor cells. The average particle size of F0, determined using Malvern instruments, measured at 229.7 nm (Fig. 5A). Assessment of size uniformity within the formulation was carried out through the polydispersity index (PDI), yielding a value of 0.296. With a PDI below 0.5, the formulation demonstrated good size homogeneity and smoothness. Moreover, the zeta potential was determined as it serves an as indicator of electrostatic interactions between particles, with values surpassing 30 mV indicative of stability and non-aggregation of carriers. The zeta potential was found to be −34.6 mV which underscored the system's robust physical stability (Fig. 5A). [74]. Dispersions with zeta potential levels larger than 30 mV (positive or negative) are supposedly considered to be relatively stable [74]. Using Zetasizer, the zeta potential of the formulation was determined. The zeta potential was observed in the range of −34 mV which indicated that the nanoparticles were strongly anionic [75]. Additionally, the morphology examination by SEM (JSM-IT100) revealed that nanocarriers exhibited uniform distribution, smooth surface texture and absence of aggregation (Fig. 5B). The formation of smooth and evenly distributed particles can be attributed to interplay of a fully saturated polymer and a controlled solvent diffusion rate, as elucidated by previous research work [65].

3.2.4. In-vitro drug release study

An important criterion to take into account for the evaluation of the effectiveness of drug carriers is the in vitro release kinetics of nanoparticles, which offers crucial information about their capacity to allow target drug release [76,77]. Prior to the site of action (cancerous cells), a tumor-targeted drug delivery system must display little or no drug release or else, the drug will be absorbed in the gastro-intestinal tract (GIT), which will reduce its effectiveness. Additionally, the prolonged and regulated release of hydrophobic medications is favored because it lessens the need for repeated drug administration and a number of its

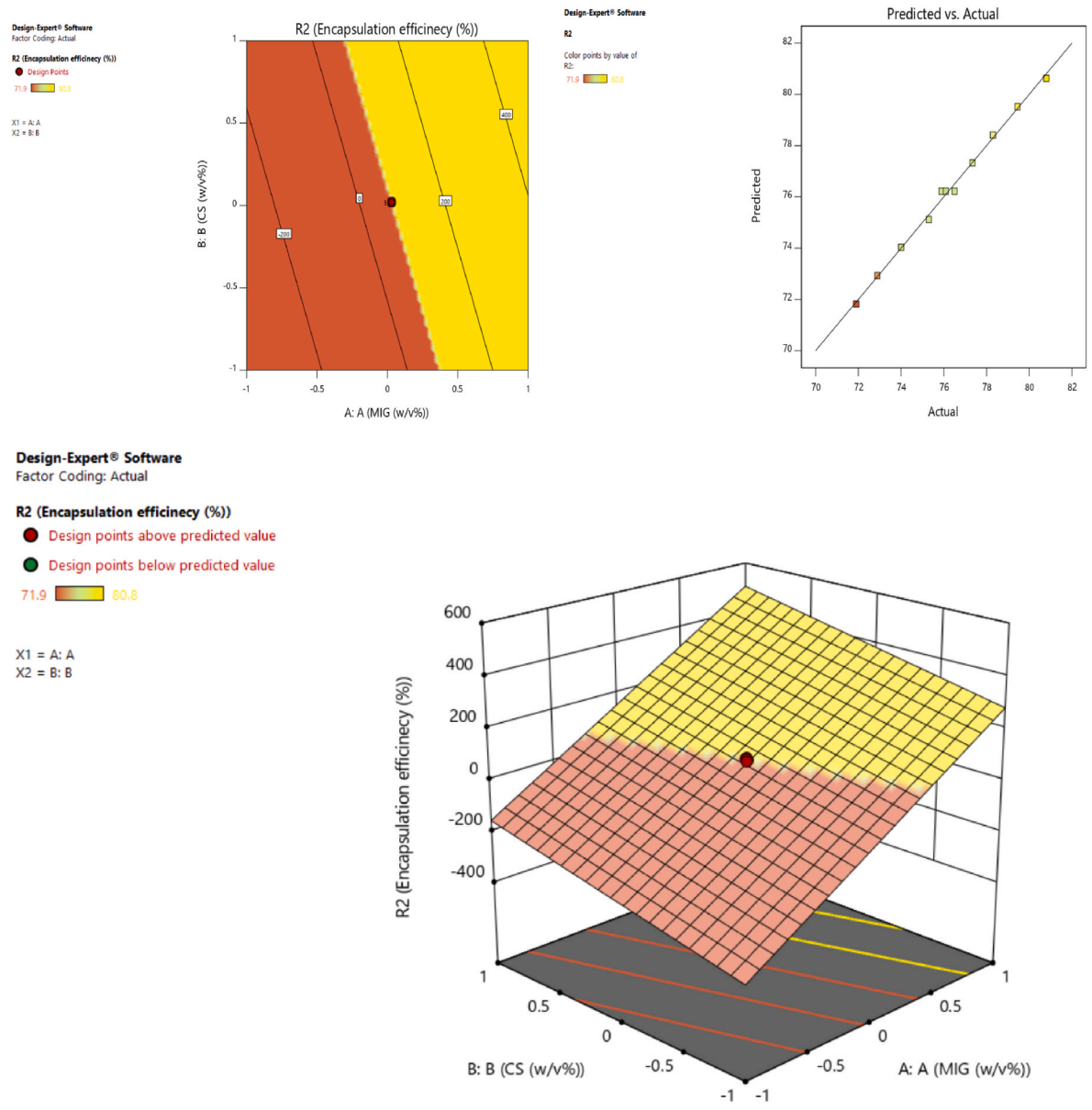

Fig. 3. 2-D contour surface predicted vs actual and 3-D response graphs illustrating the influence of MIG and CS content on DEE (%) of MIG/CS NPs.

Table 3
The optimized formulation with superlative independent variables.

Number	MIG (w/v %)	**CS (w/v%)**	PS (mm)			DEE (%)		
			Predicted value	Actual value	% error	Predicted value	Actual value	% error
F–O	0.02	0.01	231.62	229.7 ± 3.2	0.83	71.96	69.5% ± 2.0	3.5

Comparative Analysis of Various Plant gum-CS NPs with Optimized MIG-CS NPs

Nanoformulations	Particle Size (nm)	Entrapment efficiency (%)	Key characteristics	References
MTX loaded Linseed mucilage-chitosan nanoparticles	246.6	54.98 ± 1.08	pH responsive and sustained drug release strong antitumor effects against HepG2 and MCF-7 cells	[1]
Flaxsed Mucilage and chitosan nanoparticles	326	82.06	pH responsive and sustained drug release	[69]
Insulin loaded carboxymethylated iota carrageenan/chitosan NPs	Particle Size (nm)	Entrapment efficiency (%)	pH responsive and sustained drug release	[70]
Scutellarin loaded HP-b-CD-chitosan NPs	246.6	54.98 ± 1.08	Biphasic and efficacious drug release	[71]

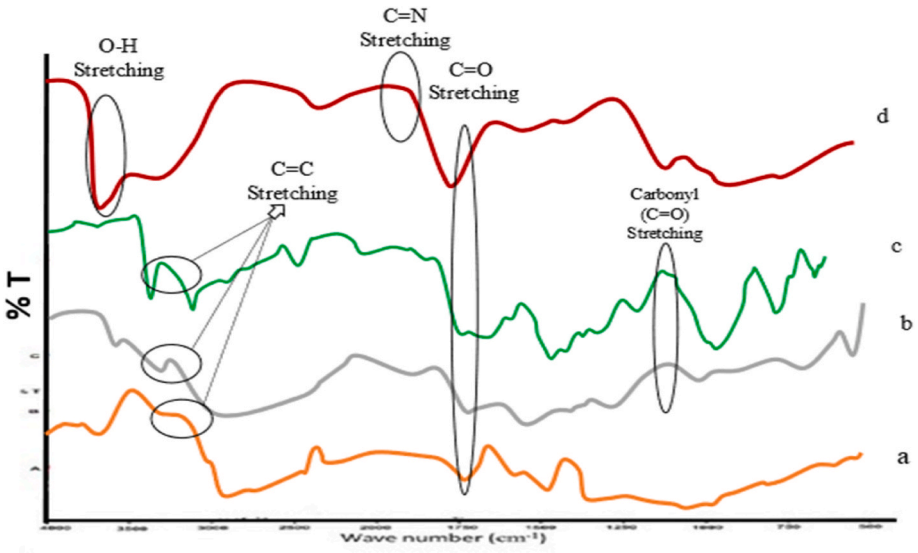

Fig. 4. Drug polymer compatibility FTIR studies a) *Mangifera indica* gum b) Methotrexate, c) Chitosan, d) Drug-loaded nanoparticles.

Table 4
Drug Encapsulation efficiency, % drug content and % yield of optimized formulation; F0.

Formulation	% Drug Encapsulation efficiency	% Drug content	% Yield
F0	69.5% ± 2.0	71.4% ± 2.0	69.7% ± 2.0

negative effects [77,78]. In simulated normal and malignant cell environment, the cumulative release of MTX from F0 was investigated (Fig. 6). The pH 1.2 was selected to mimic an acidic environment, pH 7.4 to represent an intestinal environment and 6.8 to simulate conditions in bloodstream. These pH values were chosen to align with the physiological pH variations encountered by drug carriers in patients' body. For 24 h, the release patterns of MTX from MIG-CS NPs were tested in simulated stomach fluid (SGF; pH 1.2), colonic fluid (pH 6.8), and intestinal fluid (SIF; pH 7.4). The release was found to be 26.7, 51.8 and 73.9 in pH 1.2, 6.8 and 7.4 respectively indicating that NPs allow a targeted delivery to cancer cells (Fig. 6A). Moreover, in a medium with varying pH, a biphasic release pattern was discerned for MIG-CS NPs, succeeded by a sustained release for the total drug content. This initial burst could be attributed to the amount of drug present at the surface of NPs, Conversely, the drug molecules located at core of NPs, within a densely embedded polymer matrix, contributed to the sustained release at pH of 6.8. The initial burst is considered advantageous as it allows for the rapid attainment of a therapeutic concentration, while subsequent sustained release pattern ensures an extended therapeutic effect (Fig. 6B) [79].

3.2.5. *In-vitro drug release kinetics*

To study the MTX release process from MIG-CS NPs (F0), a variety of mathematical formulas were used to incorporate the cumulative drug release (percent CDR) data. Despite the likelihood that one model will dominate in the release kinetics, a variety of models often act in concert to affect the release rate of nanocarriers. Five kinetic models were then applied to the dissolution data as a result. These include zero order, first order, Korsmeyer-Peppas model, Hixson-Crowell model, and Higuchi model. The selection of kinetic model was based on R2 obtained close to unity. In-vitro release data was put in numerous mathematical models

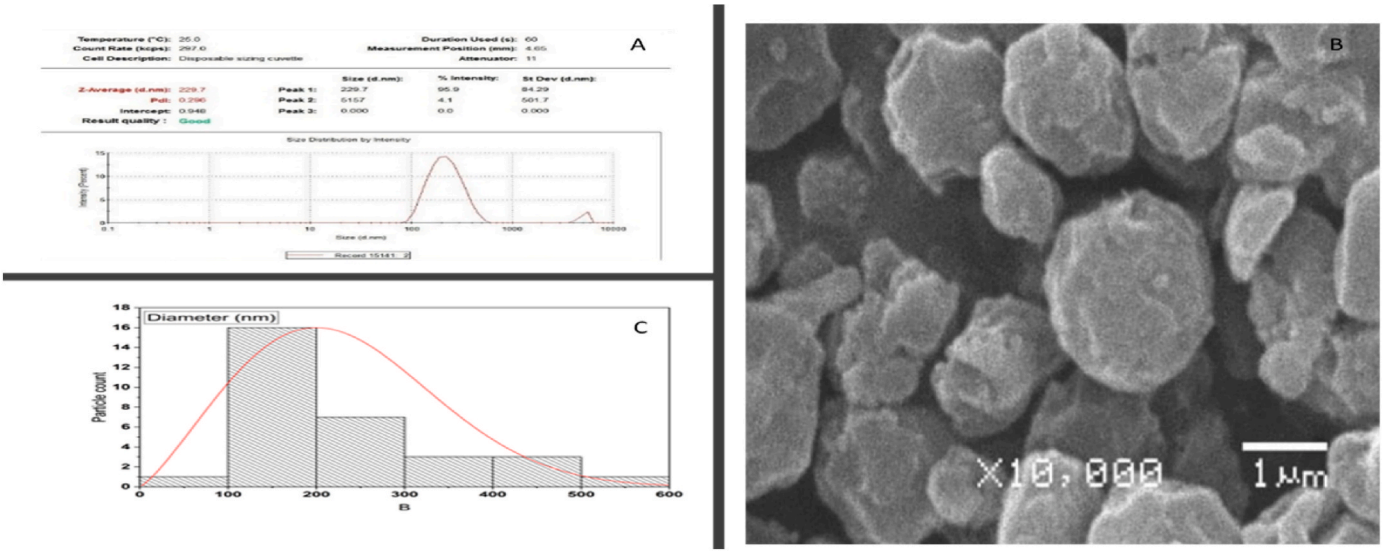

Fig. 5. A. Particle size and Zeta Potential of nanoparticles using Dynamic Light Scattering (DLS), B and C. SEM image and histogram of nanoparticles representing the particles size distribution.

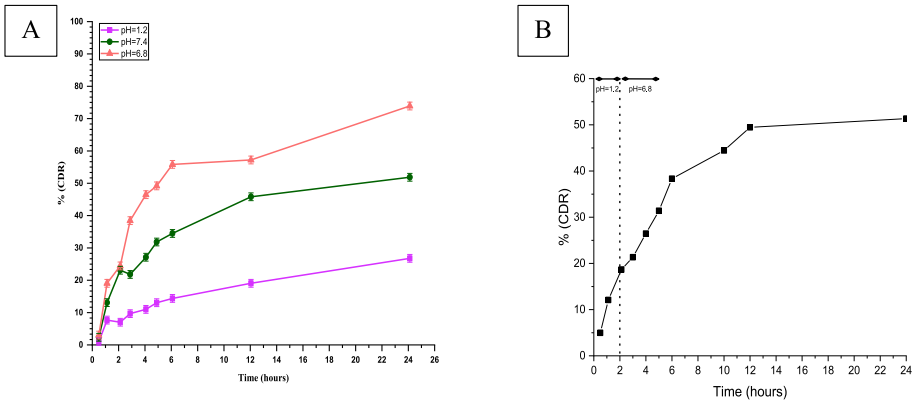

Fig. 6. MTX Release Profile of MIG-CS NPs at pH = 1.2; pH = 6.8 and pH = 7.4 A) in different mediums B) in same medium with varying pH.

using a DD solver. At all pH levels (1.2, 6.8, and 7.4), the MTX-loaded MIG-CS NPs followed the Higuchi model, with the highest R2 values compared to all other models. The R2 values were quite close to 1 (Table 5). The Higuchi model, which is frequently used to examine the drug release kinetics of NP formulations, is linked to three hypotheses. First off, drug solubility initially outweighs drug concentration. Second, because NPs are thin compared to the thickness of the preparation system, the drug particles are contained within them with no drug on their surface. Thirdly, the Higuchi model is based on porous systems, in which hydrophilic polymers quickly dissolve to form pores, drug diffusivity is constant, and drug release takes place through matrix pores.

The data was also examined using the Korsmeyer-Peppas model, which, after the Higuchi model, demonstrated the second highest R2 values. According to Korsmeyer, the mechanism of release can be inferred by including the first 60% of release data, where n is the release exponent and indicates the mechanism of drug release [80]. The geometry of the carrier and its release mechanism have an impact on the diffusional exponent n. For spherical particles, Fickian release is indicated by n 0.43 (case I transport); non-Fickian release is indicated by n 0.85; Fickian release is indicated by n 0.85 (case II transport); and super case II transport is investigated if $n > 1$. The value of n at pH 1.2, 6.8 and 7.4 was found to be less than 0.45 illustrating the Fickian release mechanism [81,82].

3.2.6. Hemolytic studies

In studies of nanocarriers interaction with blood components, one of the most frequent experiments is the determination of hemolytic characteristics [83,84]. Due to differences in experimental methods and a lack of generally recognized standards for determining the test-result validity, interpreting the results of these investigations is challenging. The majority of particle-induced hemolysis investigations conducted in vitro measure the degree of hemolysis by centrifuging intact cells after incubating the particles with blood and looking for plasma-free hemoglobin derivatives using spectrophotometry [85,86]. The incubation period, wavelength used to measure hemoglobin, and blood conditions (such as the use of purified erythrocytes rather than whole blood and the addition of various anticoagulants) differ greatly amongst studies [87]. To calculate the hemotoxic effect of F0 NPs, blank MIG-CS NPs and MTX loaded MIG-CS NPs, a hemolytic toxicity investigation was carried out at various concentrations (0.01, 0.025, 0.005, and 0.1 mg/mL). The % hemolysis ranges from 0.06% to 2.68% in blank nanoparticles in descending order of drug concentration from 0.1 to 0.01 mg/mL, while in the case of drug-loaded nanoparticles, % hemolysis was in the range of 0.07%–4.05% in the same descending order of drug concentration demonstrating that the toxicity of RBCs is reduced with increasing polymeric drug encapsulation. The comparison of different concentrations of blank and drug-loaded NPs % hemolysis is given in Fig. 7.

Table 5
Kinetic parameters of methotrexate release from formulation at various pH of 7.4, 6.8 and 1.2

Sr. No.	Model	Parameters	pH 7.4	pH 6.8	pH 1.2
1	**Zero Order**	**k0**	2.95	4.2	1.37
		R^2	0.022	−0.21	0.4614
2	**First Order**	**k1**	0.05	0.119	0.017
		R^2	0.533	0.703	0.5907
3	**Higuchi model**	**k_H**	12.31	17.8	5.54
		R^2	0.894	0.789	0.9660
4	**Korsmeyer model**	**k_{KP}**	14.88	23.23	5.5
		R^2	0.924	0.852	0.9612
		n	0.41	0.385	0.498
5	**Hixson-Crowell model**	**k_{HC}**	0.015	0.035	0.005
		R^2	0.0383	0.56	0.5493

3.2.7. In vitro cell viability via MTT assay

The MTT assay has been used to examine in-vitro cytotoxic efficacy of MTX loaded MIG-CS NPs (F0) on Hep G2 cancer cell-lines. The treatment of these cells with MTX-Loaded MIG-CS NPs, which drastically reduced their cell viability, showed that these MIG-CS NPs may efficiently kill cancer cells (Fig. 8) [14]. While comparing the MTX-loaded MIG-CS NPs to blank nanoparticles, it was shown that the activity of the latter was significantly more time- and concentration-dependent. In the first 24 h, it was seen that the MTX-loaded MIG-CS NPs were more cytotoxic than the control MIG-CS nanoparticles. In contrast to NPs, the MTX's cytotoxic effect was more pronounced in the initial 24 h. This is explained by the fact that, while just a small amount of the drug is given to cell cultures in NPs, the free

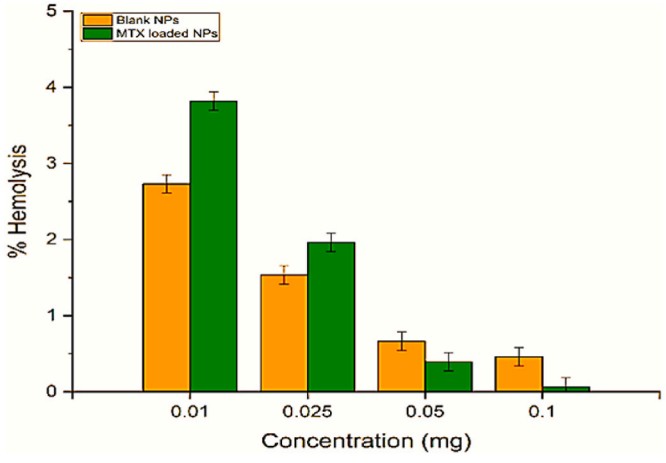

Fig. 7. % Hemolysis of blank and drug (MTX) loaded NPs.

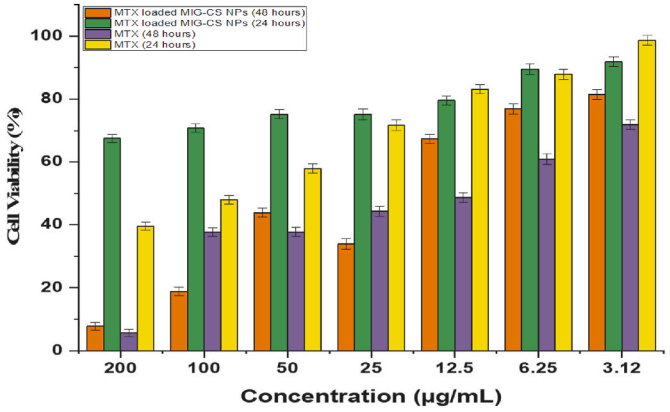

Fig. 8. % Cell viability of methotrexate-loaded MTX-Loaded MIG-CS nanoparticles.

drug is swiftly taken up by malignant cells through passive diffusion since cells are immediately available to full drug concentration. The dose of the medicine is anticipated to gradually rise until it reaches a stable level in the NPs. Therefore, after 24 h, there was a noticeable rise in the cellular toxicity of MTX-loaded NPs for cell lines [88,89]. After 48 h, both MTX and MTX loaded MIG-CS NPs dramatically reduced the rate of cell division in the cancer cell line. When compared to free MTX after 48 h, the activity of MTX loaded MIG-CS NPs caused substantial cancer cell death and dose-dependent suppression of cell growth by the anti-cancer drug without harming the healthy cells. The NPs were observed at concentrations ranging from 3.12 to 200 µg/mL, concluding that MTX loaded MIG-CS NPs can be an effective method for precise target delivery.

3.2.8. *In-vivo acute toxicity analysis*

To evaluate the cytotoxicity of drug carriers and their lethal dose levels, acute toxicity is used. In addition, a key aspect of assessing the long-term mortality data is the use of appropriate animal species for in-vivo toxicity studies. These experiments can eventually be applied to determine the sensitivity pattern of human tissue [90,91]. In vivo investigations are necessary because in vitro studies of drug dispersion and permeability cannot accurately simulate a living biological system and have other limitations. In vitro studies cannot completely predict how carrier will interact with various organs and organ systems, or how it will interact with other drugs [92]. To establish a carrier safe and effective for practical administration, in vivo acute toxicity study is required. These multifactorial in vivo results can generate a measurable set of pharmacokinetics characteristics by accounting for the interplay between drug encapsulating carrier permeability, distribution, and metabolism [93]. To assure the safety of the drug, model animal drug testing helps identify toxicities, side effects, and carrier's cellular interactions, amongst other pharmacokinetic properties.

In the present study, control and test mice groups were separately administered with an experimental dose of about 1 mg of standard mice feed and blank MIG-CS NPs respectively, followed by a week of acclimatization, lasting for 21 days. In comparison to control group, changes in body weight, mortality, survival, and other clinical parameters were noticed. However, neither mortality nor any hazardous side effects (skin colour change, tremors, and diarrhea) were noted in either group. Additionally, the mice's behavior and sleeping habits stayed the same for 14 days and no death occurred. Because no animal died during the 14-day observation period in either group, it was impossible to calculate the lethal dose. Equal amounts of food and water were consumed by both groups, however, the test group's weight appeared to have decreased slightly. Both groups consumed the same amount of food and liquids, however, the test group's weight appeared to have decreased slightly. However, compared to the animals in the control group, the difference in the weight change was not much significant. The lipid, hepatic and renal profile of test group has been shown in Table 6.

Table 6
Results of Lipid Profile, liver functioning and renal functioning testing (LPT) carried out on albino mice.

Lipid Profile Test (LPT)

Sr. no.	Test	Result (mg/dL)	Reference value (mg/dL)
1	**Serum Cholesterol**	154	Without known coronary artery disease less than or equal to 200: Desirable With known coronary artery disease less than or equal to 160: Optimal
2	**Serum Triglycerides**	110	Up to 150
3	**HDL Cholesterol**	38	Without known coronary artery disease less than or equal to 41: Desirable with known coronary artery disease less than or equal to 41: Optimal
4	**LDL Cholesterol**	94	Without known coronary artery disease less than or equal to 130: Desirable
5	**VLDL**	22	15–40

Liver Function Test (LFT)

Sr.no.	Test	Result(µ/L)	Reference value (µ/L)
1	**SGPT**	32	32-Female 40-Male
2	**SGOT**	34	32-Female 40-Male
3	**Alkaline phosphate**	195	Up to 250
4	**Bilirubin Total**	0.71 mg/dL	0.6–1 mg/dL

Renal Function Test (RFT)

Sr.no.	Test	Result (mg/dL)	Reference value (mg/dL)
1	**B. Urea**	27	20–50
2	**S. Creatinine**	0.8	0.6–1.3

Additionally, for conducting an organ functioning test in test group, blood was drawn using single-use syringes. For the preparation of histology slides of the heart, kidney, liver, stomach, small intestine of mice, all these organs were separated, removed, weighed, and fixed in Corony's fixative. The organs show no toxicity. The figures of different organ slides are shown in Fig. 9.

4. Conclusion

A modified coacervation technique was employed to encapsulate MTX within nanocarriers composed of MIG and CS. An optimization process was carried out using response surface methodology (RSM) to fine tune the experimental procedure for efficaciously synthesizing the optimized MIG/CS NPs. The optimal formulation, denoted F_0 had MIG and CS concentrations of 0.02 w/v% and 0.01% respectively. Subsequently, Fo was characterized to evaluate its potential as an effective MTX delivery carrier. FTIR analysis confirmed the successful encapsulation of MTX. Furthermore, the nanoscale size and morphology were ascertained through DLS, zeta potential measurements and SEM. Moreover, the MIG/CS NPs exhibited significant encapsulation efficiency and capacity to regulate MTX release, particularly over a 24-h period, demonstrating their effectiveness within context of tumor-relevant pH conditions (pH 6.8). Additionally, in vitro experiments employing HeP-G2 cancer cell lines indicated a significant cytotoxic response to MTX loaded MIG-CS NPs, underscoring the carrier potential for targeted cancer therapy. This investigation advocates the benefits of employing natural polymers in the encapsulation of chemotherapeutic agents, which could potentially reduce the side effects associated with cancer medications and enhance their responsiveness within the tumor microenvironment. Taking a forward-looking stance, this study suggests that the use of MTX loaded MIG-CS NPs holds a great potential in achieving precise targeting and eradication of malignant cells. This not

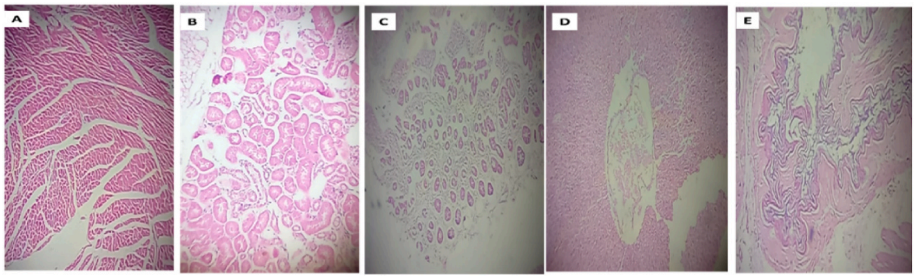

Fig. 9. Cross-sectional microscopic images of albino mice organs; a) Heart b) kidney c) small intestine d) liver. e) stomach.

only opens the door for further investigation but also lays the foundations for innovative approaches to cancer treatments using plant gum based NPS. Further research avenues may include the enhancement of pH responsive systems tailored for personalized medicine, streamlining process of scalability and delving into the dynamics of drug release mechanisms to elevate the precision and efficacy of cancer therapy.

CRediT authorship contribution statement

Sobia Noreen: Conceptualization, Designing, Supervision of the experimentation, Writing review and editing. Shazma Ehsan: Methodology, Investigation, Writing review & editing. Shazia Akram Ghumman: Methodology, Investigation, Writing review & editing. Fozia Batool: Supervision, Investigation, Writing review & editing. Sara Hasan: Methodology, Investigation, Writing review & editing. Bushra Ijaz: Methodology, Investigation, Writing review & editing. Khadeeja Ali Mohammed Alsader: Methodology, Investigation. Bahareh Shirinfar: Methodology, Investigation, Writing review & editing. Nisar Ahmed: Supervision, Designing, Writing-review & editing, Funding acquisition.

Declaration of competing interest

The authors declare that they have no known competing financial interests or personal relationships that could have appeared to influence the work reported in this paper.

Data availability

No data was used for the research described in the article.

Acknowledgment

Support from Cardiff University to Dr. Nisar Ahmed is gratefully acknowledged.

References

[1] S.A. Ghumman, A. Mahmood, S. Noreen, A. Aslam, B. Ijaz, A. Amanat, R. Kausar, M. Rana, H. Hameed, Chitosan-linseed mucilage polyelectrolyte complex nanoparticles of methotrexate: in vitro cytotoxic efficacy and toxicological studies, Arab. J. Chem. 16 (2) (2023), 104463.
[2] B.N. Cronstein, T.M. Aune, Methotrexate and its mechanisms of action in inflammatory arthritis, Nat. Rev. Rheumatol. 16 (3) (2020) 145–154.
[3] E. Akbari, H. Mousazadeh, Z. Sabet, T. Fattahi, A. Dehnad, A. Akbarzadeh, E. Alizadeh, Dual drug delivery of trapoxin a and methotrexate from biocompatible plga-peg polymeric nanoparticles enhanced antitumor activity in breast cancer cell line, J. Drug Deliv. Sci. Technol. 61 (2021), 102294.
[4] N. Kaushik, S.B. Borkar, S.K. Nandanwar, P.K. Panda, E.H. Choi, N.K. Kaushik, Nanocarrier cancer therapeutics with functional stimuli-responsive mechanisms, J. Nanobiotechnol. 20 (1) (2022) 1–23.
[5] X. Zhao, J. Bai, W. Yang, Stimuli-responsive nanocarriers for therapeutic applications in cancer, Cancer. Biol. Med. 18 (2) (2021) 319.
[6] A. Eftekhari, C. Kryschi, D. Pamies, S. Gulec, E. Ahmadian, D. Janas, S. Davaran, R. Khalilov, Natural and synthetic nanovectors for cancer therapy, Nanotheranostics 7 (3) (2023) 236.
[7] M. Moradi Pour, R. Saberi Riseh, Y.A. Skorik, Sodium alginate–gelatin nanoformulations for encapsulation of bacillus velezensis and their use for biological control of pistachio gummosis, Materials 15 (6) (2022) 2114.
[8] R. Saberi Riseh, M. Ebrahimi-Zarandi, E. Tamanadar, M. Moradi Pour, V.K. Thakur, Salinity stress: toward sustainable plant strategies and using plant growth-promoting rhizobacteria encapsulation for reducing it, Sustainability 13 (22) (2021), 12758.
[9] W.H. De Jong, P.J. Borm, Drug delivery and nanoparticles: applications and hazards, Int. J. Nanomed. 3 (2) (2008) 133–149.
[10] M.R. Saboktakin, R.M. Tabatabaie, A. Maharramov, M.A. Ramazanov, Synthesis and in vitro evaluation of carboxymethyl starch–chitosan nanoparticles as drug delivery system to the colon, Int. J. Biol. Macromol. 48 (3) (2011) 381–385.
[11] A. Nasibova, Generation of nanoparticles in biological systems and their application prospects, Adv. Biol. Earth Sci 8 (2023) 140–146.
[12] R. Khalilov, A comprehensive review of advanced nano-biomaterials in regenerative medicine and drug delivery, Advances in Biology & Earth Sciences 8 (1) (2023).
[13] S. Mohan, O.S. Oluwafemi, N. Kalarikkal, S. Thomas, S.P. Songca, Biopolymers–application in nanoscience and nanotechnology, Recent Adv. Biopolym. 1 (1) (2016) 47–66.
[14] S. Noreen, S. Hasan, S.A. Ghumman, S.N.A. Bukhari, B. Ijaz, H. Hameed, H. Iqbal, A. Aslam, M.A.M. Elsherif, S. Noureen, Ph responsive abelmoschus esculentus mucilage and administration of methotrexate: in-vitro antitumor and in-vivo toxicity evaluation, Int. J. Mol. Sci. 23 (5) (2022) 2725.
[15] Y. Wang, W. Qu, S. Choi, Fda's Regulatory Science Program for Generic Pla/plga-Based Drug Products, American Pharmaceutical Review, 2019.
[16] J. Zhou, K. Hirota, R. Ackermann, J. Walker, Y. Wang, S. Choi, A. Schwendeman, S. P. Schwendeman, Reverse engineering the 1-month lupron depot®, AAPS J. 20 (2018) 1–13.
[17] P.D. Choudhary, H.A. Pawar, Recently investigated natural gums and mucilages as pharmaceutical excipients: an overview, J. Pharm. 2014 (2014).
[18] Z.U. Khan, T. Khan, A. Mannan, A. Ali, J. Ni, In vitro and ex vivo evaluation of mangifera indica l. Extract-loaded green nanoparticles in topical emulsion against oxidative stress and aging, Biomedicines 10 (9) (2022) 2266.
[19] K. Zhou, L. Su, L. Yu, Phytochemicals and antioxidant properties in wheat bran, J. Agric. Food Chem. 52 (20) (2004) 6108–6114.
[20] R.S. Riseh, E. Tamanadar, M.M. Pour, V.K. Thakur, Novel approaches for encapsulation of plant probiotic bacteria with sustainable polymer gums: application in the management of pests and diseases, Adv. Polym. Technol. 2022 (2022).
[21] K.N. Thakkar, S.S. Mhatre, R.Y. Parikh, Biological synthesis of metallic nanoparticles, Nanomed. Nanotechnol. Biol. Med. 6 (2) (2010) 257–262.
[22] H.M. Masroor, M.A. Anjum, S. Hussain, S. Ejaz, S. Ahmad, S. Ercisli, M. Zia-Ul-Haq, Zinc ameliorates fruit yield and quality of mangoes cultivated in calcareous soils, Erwerbsobstbau 58 (1) (2016).
[23] E.S.Y. Ahmed, E.S.E. Abbas, Extraction and evaluation of mangifera indica gum as a sustained release polymer in glibenclamide matrix tablets, Pharmaceut. Biosci. J. (2018), 01-06.
[24] A.J. Núñez Sellés, H.T. Vélez Castro, J. Agüero-Agüero, J. González-González, F. Naddeo, F. De Simone, L. Rastrelli, Isolation and quantitative analysis of phenolic antioxidants, free sugars, and polyols from mango (mangifera indica l.) stem bark aqueous decoction used in Cuba as a nutritional supplement, J. Agric. Food Chem. 50 (4) (2002) 762–766.
[25] A.K. Singh, V.K. Shingala, R.P. Selvam, T. Sivakumar, Evaluation of mangifera indica gum as tablet binder, Int. J. Pharm. Tech. Res. 2 (3) (2010) 2098–2100.
[26] J. Yang, M. Shen, Y. Luo, T. Wu, X. Chen, Y. Wang, J. Xie, Advanced applications of chitosan-based hydrogels: from biosensors to intelligent food packaging system, Trends Food Sci. Technol. 110 (2021) 822–832.
[27] R.S. Riseh, M. Hassanisaadi, M. Vatankhah, S.A. Babaki, E.A. Barka, Chitosan as potential natural compound to manage plant diseases, Int. J. Biol. Macromol. (2022).
[28] F. Garavand, I. Cacciotti, N. Vahedikia, A. Rehman, Ö. Tarhan, S. Akbari-Alavijeh, R. Shaddel, A. Rashidinejad, M. Nejatian, S. Jafarzadeh, A comprehensive review on the nanocomposites loaded with chitosan nanoparticles for food packaging, Crit. Rev. Food Sci. Nutr. 62 (5) (2022) 1383–1416.
[29] Z. Deng, T. Wang, X. Chen, Y. Liu, Applications of chitosan-based biomaterials: a focus on dependent antimicrobial properties, Marine Life Sci. Technol. 2 (2020) 398–413.
[30] R.S. Riseh, E. Tamanadar, N. Hajabdollahi, M. Vatankhah, V.K. Thakur, Y. A. Skorik, Chitosan microencapsulation of rhizobacteria for biological control of plant pests and diseases: recent advances and applications, Rhizosphere (2022), 100565.

[31] S.-Y. Kwak, T.T.S. Lew, C.J. Sweeney, V.B. Koman, M.H. Wong, K. Bohmert-Tatarev, K.D. Snell, J.S. Seo, N.-H. Chua, M.S. Strano, Chloroplast-selective gene delivery and expression in planta using chitosan-complexed single-walled carbon nanotube carriers, Nat. Nanotechnol. 14 (5) (2019) 447–455.
[32] D.S. Salem, S.A. Shouman, Y. Badr, Laser-triggered release of drug encapsulated in chitosan nanoparticles for therapy of hepatocellular carcinoma, in: Colloidal Nanoparticles for Biomedical Applications XIV, SPIE, 2019.
[33] S.L. Patwekar, A.P. Potulwar, S.R. Pedewad, M.S. Gaikwad, S. Khan, A. Suryawanshi, Review on polyelectrolyte complex as novel approach for drug delivery system, Int. J. Pharm. Pharmaceut. Res. 5 (2016) 98–109.
[34] J. Potaś, E. Szymańska, K. Winnicka, Challenges in developing of chitosan–based polyelectrolyte complexes as a platform for mucosal and skin drug delivery, Eur. Polym. J. 140 (2020), 110020.
[35] R. Saberi Riseh, M. Ebrahimi-Zarandi, M. Gholizadeh Vazvani, Y.A. Skorik, Reducing drought stress in plants by encapsulating plant growth-promoting bacteria with polysaccharides, Int. J. Mol. Sci. 22 (23) (2021), 12979.
[36] C. Sebaaly, A. Trifan, E. Sieniawska, H. Greige-Gerges, Chitosan-coating effect on the characteristics of liposomes: a focus on bioactive compounds and essential oils: a review, Processes 9 (3) (2021) 445.
[37] P. Chakraborty, U. Chaurasia, D.D. Chakraborty, I. Chanda, Polysaccharide-based Nanoparticles for the Enhanced Delivery of Poorly Soluble Drugs *Polysaccharide-Based Nano-Biocarrier in Drug Delivery*, CRC Press, 2018, pp. 129–151.
[38] J.H. Hamman, Chitosan based polyelectrolyte complexes as potential carrier materials in drug delivery systems, Mar. Drugs 8 (4) (2010) 1305–1322.
[39] C. He, Y. Guo, B. Karmakar, A. El-kott, A.E. Ahmed, A. Khames, Decorated silver nanoparticles on biodegradable magnetic chitosan/starch composite: investigation of its cytotoxicity, antioxidant and anti-human breast cancer properties, J. Environ. Chem. Eng. 9 (6) (2021), 106393.
[40] R. Vinod, Formulation and evaluation of nicorandil sustained release matrix tablets using natural gum mangifera indica as release modifier, Asian J. Biomed. Pharmaceut. Sci. 3 (18) (2013) 54.
[41] R. Malviya, S. Raj, S. Fuloria, V. Subramaniyan, K. Sathasivam, U. Kumari, D. U. Meenakshi, O. Porwal, D.H. Kumar, A. Singh, Evaluation of antitumor efficacy of chitosan-tamarind gum polysaccharide polyelectrolyte complex stabilized nanoparticles of simvastatin, Int. J. Nanomed. 16 (2021) 2533.
[42] S. Javed, W. Ahsan, S. Talegaonkar, F. Ahmad, P fabrication and characterization of minocycline loaded chitosan microspheres by central composite design for the local delivery in periodontal pockets, Acta Pol. Pharm. 78 (5) (2021) 679–691.
[43] M.E. Rao, S. Swain, C.N. Patra, S.P. Mund, Formulation design, optimization and characterization of eprosartan mesylate nanoparticles, Nanosci. Nanotechnol. - Asia 8 (1) (2018) 130–143.
[44] M. Danaei, M. Dehghankhold, S. Ataei, F. Hasanzadeh Davarani, R. Javanmard, A. Dokhani, S. Khorasani, M. Mozafari, Impact of particle size and polydispersity index on the clinical applications of lipidic nanocarrier systems, Pharmaceutics 10 (2) (2018) 57.
[45] R. Malviya, S. Raj, S. Fuloria, V. Subramaniyan, K. Sathasivam, U. Kumari, D. Unnikrishnan Meenakshi, O. Porwal, D. Hari Kumar, A. Singh, Evaluation of antitumor efficacy of chitosan-tamarind gum polysaccharide polyelectrolyte complex stabilized nanoparticles of simvastatin, Int. J. Nanomed. (2021) 2533–2553.
[46] S. Noureen, S. Noreen, S.A. Ghumman, F. Batool, H. Hameed, S. Hasan, F. Noreen, M.A. Elsherif, S.N.A. Bukhari, Prunus armeniaca gum-alginate polymeric microspheres to enhance the bioavailability of tramadol hydrochloride: formulation and evaluation, Pharmaceutics 14 (5) (2022) 916.
[47] E. Farrell, J.-L. Brousseau, Guide for dls sample preparation, Brookhaven Instrum 1 (631) (2014) 1–3.
[48] A.J. Shinde, N. Harinath, Formulation, development and characterization of simvastatin nanoparticles by solvent displacement method, Der Pharm. Lett. 6 (2) (2014) 145–155.
[49] R. Saberi Riseh, M. Moradi Pour, E. Ait Barka, A novel route for double-layered encapsulation of streptomyces fulvissimus uts22 by alginate–Arabic gum for controlling of pythium aphanidermatum in cucumber, Agronomy 12 (3) (2022) 655.
[50] M. Moradi-Pour, R. Saberi-Riseh, K. Esmaeilzadeh-Salestani, R. Mohammadinejad, E. Loit, Evaluation of bacillus Velezensis for Biological Control of Rhizoctonia Solani in Bean by Alginate/gelatin Encapsulation Supplemented with Nanoparticles, 2021.
[51] T. Gomathi, C. Govindarajan, M.H.R. Hr, P. Sudha, P.M. Imran, J. Venkatesan, S.-K. Kim, Studies on drug-polymer interaction, in vitro release and cytotoxicity from chitosan particles excipient, Int. J. Pharm. 468 (1–2) (2014) 214–222.
[52] S. Bashir, M. Aamir, R.M. Sarfaraz, Z. Hussain, M.U. Sarwer, A. Mahmood, M. R. Akram, M.N. Qaisar, Fabrication, characterization and in vitro release kinetics of tofacitinib-encapsulated polymeric nanoparticles: a promising implication in the treatment of rheumatoid arthritis, Int. J. Polym. Mater. Polym. Biomater. 70 (7) (2021) 449–458.
[53] F.M. Almutairi, H.A. El Rabey, A.A. Tayel, A.I. Alalawy, M.A. Al-Duais, M.I. Sakran, N.S. Zidan, Augmented anticancer activity of curcumin loaded fungal chitosan nanoparticles, Int. J. Biol. Macromol. 155 (2020) 861–867.
[54] J. Zheng, K. Nagashima, D. Parmiter, J. de la Cruz, A.K. Patri, Sem x-ray microanalysis of nanoparticles present in tissue or cultured cell thin sections, Charact. Nanopart. Intended Drug Delivery (2011) 93–99.
[55] S. Gooneh-Farahani, S.M. Naghib, M.R. Naimi-Jamal, A novel and inexpensive method based on modified ionic gelation for ph-responsive controlled drug release of homogeneously distributed chitosan nanoparticles with a high encapsulation efficiency, Fibers Polym. 21 (2020) 1917–1926.
[56] S. Flanary, A.S. Hoffman, P.S. Stayton, Antigen delivery with poly (propylacrylic acid) conjugation enhances mhc-1 presentation and t-cell activation, Bioconjugate Chem. 20 (2) (2009) 241–248.
[57] H.K. Stulzer, M.P. Tagliari, A.L. Parize, M.A.S. Silva, M.C.M. Laranjeira, Evaluation of cross-linked chitosan microparticles containing acyclovir obtained by spray-drying, Mater. Sci. Eng. C 29 (2) (2009) 387–392.
[58] A. Aluigi, M. Ballestri, A. Guerrini, G. Sotgiu, C. Ferroni, F. Corticelli, M. B. Gariboldi, E. Monti, G. Varchi, Organic solvent-free preparation of keratin nanoparticles as doxorubicin carriers for antitumour activity, Mater. Sci. Eng. C 90 (2018) 476–484.
[59] M.H. Abolhasani, M. Safavi, M.T. Goodarzi, S.M. Kassaee, M. Azin, Identification and anti-cancer activity in 2d and 3d cell culture evaluation of an iranian isolated marine microalgae picochlorum sp. Rcc486, Daru 26 (2018) 105–116.
[60] S. Batool, S. Batool, S. Shameem, F. Khalid, T. Batool, S. Yasmeen, S. Batool, Atrazine induced histopathological alterations in the liver of adult male mice, Punjab Univ. J. Zool. 36 (2) (2021) 165–170.
[61] S.A. Ghumman, A. Mahmood, S. Noreen, M. Rana, H. Hameed, B. Ijaz, S. Hasan, A. Aslam, M.F. ur Rehman, Formulation and evaluation of quince seeds mucilage–sodium alginate microspheres for sustained delivery of cefixime and its toxicological studies, Arab. J. Chem. 15 (6) (2022), 103811.
[62] A. Rehman, S.M. Jafari, Q. Tong, T. Riaz, E. Assadpour, R.M. Aadil, S. Niazi, I. M. Khan, Q. Shehzad, A. Ali, Drug nanodelivery systems based on natural polysaccharides against different diseases, Adv. Colloid Interface Sci. 284 (2020), 102251.
[63] F. Liu, X. Liang, X. Li, Z. Jiang, Self-assembled nanoparticle-based systems, Bio. Delivery Syst. Lipophilic Nutraceut.: Formulat. Fabricat. Appl. (19) (2023) 444.
[64] M.A. Bezerra, R.E. Santelli, E.P. Oliveira, L.S. Villar, L.A. Escaleira, Response surface methodology (rsm) as a tool for optimization in analytical chemistry, Talanta 76 (5) (2008) 965–977.
[65] N.R. Naveen, M. Kurakula, B. Gowthami, Process optimization by response surface methodology for preparation and evaluation of methotrexate loaded chitosan nanoparticles, Mater. Today: Proc. 33 (2020) 2716–2724.
[66] S. Noreen, S. Hasan, S.A. Ghumman, S. Anwar, H.Y. Gondal, F. Batool, S. Noureen, Formulation, statistical optimization, and in vivo pharmacodynamics of cydonia oblonga mucilage/alginate mucoadhesive microspheres for the delivery of metformin hcl, ACS Omega (2023).
[67] M. Ahuja, A. Kumar, Gum ghatti–chitosan polyelectrolyte nanoparticles: preparation and characterization, Int. J. Biol. Macromol. 61 (2013) 411–415.
[68] B. Vishwa, A. Moin, D. Gowda, S.M. Rizvi, W.A. Hegazy, A.S. Abu Lila, E.-S. Khafagy, A.N. Allam, Pulmonary targeting of inhalable moxifloxacin microspheres for effective management of tuberculosis, Pharmaceutics 13 (1) (2021) 79.
[69] M. Bhatia, S. Lohan, Flax seed mucilage-chitosan polyelectrolyte complex nanoparticles: optimization, characterization and evaluation, ACTA Pharmaceutica Sciencia 57 (3) (2019).
[70] P. Sahoo, K.H. Leong, S. Nyamathulla, Y. Onuki, K. Takayama, L.Y. Chung, Optimization of ph-responsive carboxymethylated iota-carrageenan/chitosan nanoparticles for oral insulin delivery using response surface methodology, React. Funct. Polym. 119 (2017) 145–155.
[71] S. Liu, P.C. Ho, Formulation optimization of scutellarin-loaded hp-β-cd/chitosan nanoparticles using response surface methodology with box–behnken design, Asian J. Pharm. Sci. 12 (4) (2017) 378–385.
[72] A. Hooda, A. Nanda, M. Jain, V. Kumar, P. Rathee, Optimization and evaluation of gastroretentive ranitidine hcl microspheres by using design expert software, Int. J. Biol. Macromol. 51 (5) (2012) 691–700.
[73] M.d.J. Perea-Flores, H.F. Aguilar-Morán, G. Calderón-Domínguez, A.B. García-Hernández, M. Díaz-Ramírez, H.E. Romero-Campos, A.D.J. Cortés-Sánchez, M. Salgado-Cruz, Entrapment efficiency (ee) and release mechanism of rhodamine b encapsulated in a mixture of chia seed mucilage and sodium alginate, Appl. Sci. 13 (2) (2023) 1213.
[74] M. Barani, M. Reza Hajinezhad, S. Sargazi, M. Zeeshan, A. Rahdar, S. Pandey, M. Khatami, F. Zargari, Simulation, in vitro, and in vivo cytotoxicity assessments of methotrexate-loaded ph-responsive nanocarriers, Polymers 13 (18) (2021) 3153.
[75] J.R. Varma, T.S. Kumar, B. Prasanthi, J.V. Ratna, Formulation and characterization of pyrazinamide polymeric nanoparticles for pulmonary tuberculosis: efficiency for alveolar macrophage targeting, Indian J. Pharmaceut. Sci. 77 (3) (2015) 258.
[76] B. Tian, S. Liu, W. Lu, L. Jin, Q. Li, Y. Shi, C. Li, Z. Wang, Y. Du, Construction of ph-responsive and up-conversion luminescent nayf4: Yb3+/er3+@ sio2@ pmaa nanocomposite for colon targeted drug delivery, Sci. Rep. 6 (1) (2016), 21335.
[77] T.D. Carrillo-Castillo, J.S. Castro-Carmona, A. Luna-Velasco, E.A. Zaragoza-Contreras, Ph-responsive polymer micelles for methotrexate delivery at tumor microenvironments, E-Polymers 20 (1) (2020) 624–635.
[78] B. Tian, S. Liu, W. Lu, L. Jin, Q. Li, Y. Shi, C. Li, Z. Wang, Y. Du, Construction of ph-responsive and up-conversion luminescent nayf4: Yb3+/er3+@ sio2@ pmaa nanocomposite for colon targeted drug delivery, Sci. Rep. 6 (1) (2016) 1–11.
[79] N. Ahmad, R. Ahmad, M.A. Alam, F.J. Ahmad, Enhancement of oral bioavailability of doxorubicin through surface modified biodegradable polymeric nanoparticles, Chem. Cent. J. 12 (2018) 1–14.
[80] G. Singhvi, M. Singh, In-vitro drug release characterization models, Int. J. Pharm. Stud. Res. 2 (1) (2011) 77–84.
[81] S. Azadi, H. Ashrafi, A. Azadi, Mathematical modeling of drug release from swellable polymeric nanoparticles, J. Appl. Pharmaceut. Sci. 7 (2017) 125–133.
[82] P.P. Di Mauro, Development of Novel and Multifunctional Polymeric Nanoparticles for Brain Targeted Drug Delivery, Universitat Ramon Llull, 2015.

[83] A. Brownlie, I. Uchegbu, A. Schätzlein, Pei-based vesicle-polymer hybrid gene delivery system with improved biocompatibility, Int. J. Pharm. 274 (1–2) (2004) 41–52.
[84] H.-P. Zobel, F. Stieneker, S.A.-A. Aziz, M. Gilbert, D. Werner, C.R. Noe, J. Kreuter, A. Zimmer, Evaluation of aminoalkylmethacrylate nanoparticles as colloidal drug carrier systems. Part ii: characterization of antisense oligonucleotides loaded copolymer nanoparticles, Eur. J. Pharm. Biopharm. 48 (1) (1999) 1–12.
[85] D. Guowei, K. Adriane, X. Chen, C. Jie, L. Yinfeng, Pvp magnetic nanospheres: biocompatibility, in vitro and in vivo bleomycin release, Int. J. Pharm. 328 (1) (2007) 78–85.
[86] M. Schubert, C. Müller-Goymann, Characterisation of surface-modified solid lipid nanoparticles (sln): influence of lecithin and nonionic emulsifier, Eur. J. Pharm. Biopharm. 61 (1–2) (2005) 77–86.
[87] M.A. Dobrovolskaia, J.D. Clogston, B.W. Neun, J.B. Hall, A.K. Patri, S.E. McNeil, Method for analysis of nanoparticle hemolytic properties in vitro, Nano Lett. 8 (8) (2008) 2180–2187.
[88] R. Agabeigi, S.H. Rasta, M. Rahmati-Yamchi, R. Salehi, E. Alizadeh, Novel chemo-photothermal therapy in breast cancer using methotrexate-loaded folic acid conjugated au@ sio 2 nanoparticles, Nanoscale Res. Lett. 15 (2020) 1–14.
[89] D.R. Nogueira, L. Tavano, M. Mitjans, L. Pérez, M.R. Infante, M.P. Vinardell, In vitro antitumor activity of methotrexate via ph-sensitive chitosan nanoparticles, Biomaterials 34 (11) (2013) 2758–2772.
[90] P. Abasian, M. Radmansouri, M.H. Jouybari, M.V. Ghasemi, A. Mohammadi, M. Irani, F.S. Jazi, Incorporation of magnetic nax zeolite/dox into the pla/chitosan nanofibers for sustained release of doxorubicin against carcinoma cells death in vitro, Int. J. Biol. Macromol. 121 (2019) 398–406.
[91] J.S. Maziero, V.C. Thipe, S.O. Rogero, A.K. Cavalcante, K.C. Damasceno, M. B. Ormenio, G.A. Martini, J.G. Batista, W. Viveiros, K.K. Katti, Species-specific in vitro and in vivo evaluation of toxicity of silver nanoparticles stabilized with gum Arabic protein, Int. J. Nanomed. 15 (2020) 7359.
[92] K. Brake, A. Gumireddy, A. Tiwari, H. Chauhan, D. Kumari, In vivo studies for drug development via oral delivery: challenges, animal models and techniques, Pharm. Anal. Acta 8 (2017) 560, https://doi.org/10.4172/2153-2435.1000560, volume 8• issue 8• 1000560 pharm anal acta, an open access journal issn: 2153-2435. vitro research.
[93] F. Sewell, M. Aggarwal, G. Bachler, A. Broadmeadow, N. Gellatly, E. Moore, S. Robinson, M. Rooseboom, A. Stevens, C. Terry, The current status of exposure-driven approaches for chemical safety assessment: a cross-sector perspective, Toxicology 389 (2017) 109–117.